Check for updates

Blue Emissive *fac/mer*-Iridium (III) NHC Carbene Complexes and their Application in OLEDs

Muazzam Idris, Savannah C. Kapper, Abegail C. Tadle, Thilini Batagoda, Daniel Sylvinson Muthiah Ravinson, Opeoluwa Abimbola, Peter I. Djurovich, Jongchan Kim, Caleb Coburn, Stephen R. Forrest,* and Mark E. Thompson*

The photophysical and electrochemical properties of N-heterocyclic carbene complexes of Iridium (III) (Ir(C^C:)$_3$, where C^C: = N-phenyl,N-methyl-pyrazinoimidazol-2-yl (pmpz), N,N-di-p-tolyl-pyrazinoimidazol-2-yl (tpz)) are reported. Facial and meridional isomers of Ir(pmpz)$_3$ are prepared, but only the facial isomer can be isolated for Ir(tpz)$_3$. The *fac*-Ir(pmpz)$_3$ and *fac*-Ir(tpz)$_3$ complexes have emission maxima at 465 nm in polystyrene, whereas the emission maximum of *mer*-Ir(pmpz)$_3$ is redshifted to 495 nm. The emission energies and photoluminescent quantum yield (Φ_{PL}) in solution decrease on going from nonpolar to polar solvents; however, all the complexes are efficient emitters in polystyrene at room temperature (Φ_{PL} = 88–96%) and 77 K. Blue phosphorescent organic light emitting diodes employing *fac*-Ir(tpz)$_3$ as an emissive dopant achieves a high external electroluminescence efficiency (≈18 ± 1%) and brightness (29 000 cd m^{-2}) at low current density.

1. Introduction

Organic light emitting diodes (OLEDs) have attracted considerable attention for full color displays and solid-state lighting.[1] This interest is due in large part to the development of

Dr. M. Idris, S. C. Kapper, A. C. Tadle, Dr. T. Batagoda,
D. S. Muthiah Ravinson, Prof. P. I. Djurovich, Prof. M. E. Thompson
Department of Chemistry
University of Southern California
Los Angeles, CA 90089, USA
E-mail: met@usc.edu

O. Abimbola
Department of Chemical Engineering
University of Southern California
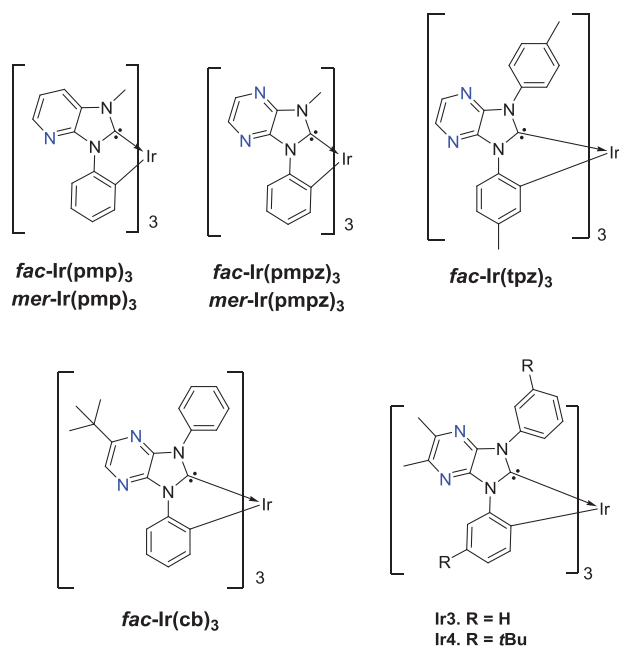Los Angeles, CA 90089, USA

J. Kim, Prof. S. R. Forrest
Department of Electrical and Computer Engineering
University of Michigan
Ann Arbor, MI 48109, USA
E-mail: stevefor@umich.edu

Dr. C. Coburn, Prof. S. R. Forrest
Department of Physics
University of Michigan
Ann Arbor, MI 48109, USA

Prof. S. R. Forrest
Department of Materials Science and Engineering
University of Michigan
Ann Arbor, MI 48109, USA

The ORCID identification number(s) for the author(s) of this article can be found under https://doi.org/10.1002/adom.202001994.

transition metal complexes as phosphorescent emitters, making it possible to harvest both singlet and triplet excitons leading to 100% electroluminescence quantum efficiency.[2] Cyclometalated iridium(III) complexes have emerged as one of the most promising triplet emitters because of their versatile color tunability, chemical stability, good thermal properties, and high photoluminescent quantum yields (Φ_{PL}).[3–7] These phosphors often involve an octahedral Ir^{3+} ion with bidentate ligands, C^N:, comprised of a covalently bonded aryl moiety and a datively bonded nitrogen group, such as pyridyl, to give a tris-cyclometalated complex, Ir(C^N:)$_3$. While efficient OLEDs using red and green Ir-based phosphorescent emitters are commercially viable,[8–10] the stability of OLEDs using blue-emitting transition metal containing complexes are presently insufficient for practical applications.[11]

Recently cyclometalated N-heterocyclic carbene (NHC)–Ir based chromophores, Ir(C^C:)$_3$, have attracted attention due to their promising properties as blue emitters.[12–19] These C^C: based emitters have an aryl group as do C^N: ligands, but utilize a carbene in place of the nitrogen basic moiety. Our group reported one of the first blue-emitting Ir–carbene complexes for OLEDs, using N-phenyl, N-methyl-imidazol-2-yl (pmi) and N-phenyl, N-methyl-benzimidazol-2-yl (pmb) ligands.[16] Since then, several homoleptic[20–23] and heteroleptic[18] derivatives of these complexes have also been reported. These Ir(C^C:)$_3$ complexes have advantages over blue emissive Ir(C^N:)$_3$ complexes as they do not suffer from deactivation of the excited state via thermal population of triplet metal-centered (^{3}MC) states, which can severely diminish their Φ_{PL}. Replacing the nitrogen basic moiety in the C^N: ligand with a strong field carbene ligand, largely mitigates this problem by destabilizing the ^{3}MC states, which makes them thermally inaccessible. Interestingly, it was found that even when the ^{3}MC states are thermally populated, the carbene iridium complexes were able to undergo reversible population of the radiative state leaving the Ir–carbene bond intact.[24] Since the Ir–N bond dissociation in the excited state has been shown to be problematic in Ir(C^N:)$_3$ complexes,[4] computational results have suggested that replacement with the stronger Ir—C carbene bond will result in a more robust emitter.[24,25]

Further work on Ir(C^C:)$_3$ complexes led to the use of the electrophilic N-phenyl, N-methyl-pyridylimidazol-2-yl ligand

Scheme 1. Structure of Ir(C^C:)$_3$ complexes.

the lowest unoccupied molecular orbital (LUMO) energies of these complexes are relatively shallow, impeding electron injection, and transport into the emissive layers. Here we investigate Ir(III) complexes employing two different N-aryl, N-aryl/methyl-pyrazinoimidazol-2-yl carbene ligands, i.e., Ir(pmpz)$_3$ and Ir(tpz)$_3$ (Scheme 1), that have deeper LUMO energy levels and lower emission energies than their pyridyl analogs. These compounds are closely related to three other reported Ir(C^C:)$_3$ complexes, Ir3 and Ir4[13] and fac-Ir(cb)$_3$[26,27] (Scheme 1). Emission from fac-Ir(pmpz)$_3$ and fac-Ir(tpz)$_3$ in comparable solvents is redshifted relative to Ir3 and Ir4; however, the former complexes have significantly higher photoluminescent quantum yields. The photophysical properties of fac-Ir(tpz)$_3$ are comparable to fac-Ir(cb)$_3$ doped at 2% in polymethylmethacrylate (PMMA) films[28] but emission is slightly red-shifted, which allows for the use of more stable hosts. Syntheses of these new materials, their chemical stability and properties (electrochemical, photophysical, and electroluminescent) are discussed.

2. Results and Discussion

2.1. Synthesis

Synthesis of mer-Ir(pmpz)$_3$ is accomplished in four steps (**Scheme 2**). Methylation of the pyrazinoimidazole in the third step yielded two regioisomers, one with the desired methylation on the imidazole nitrogen and the other methylated on one of the pyrazino nitrogens. The ratio of the desired to undesired products is roughly 1:1. Unfortunately, separation of the two components by crystallization or chromatography proved problematic; thus the isomeric mixture that was 50% pure product was used in the final step—cyclometallation of the
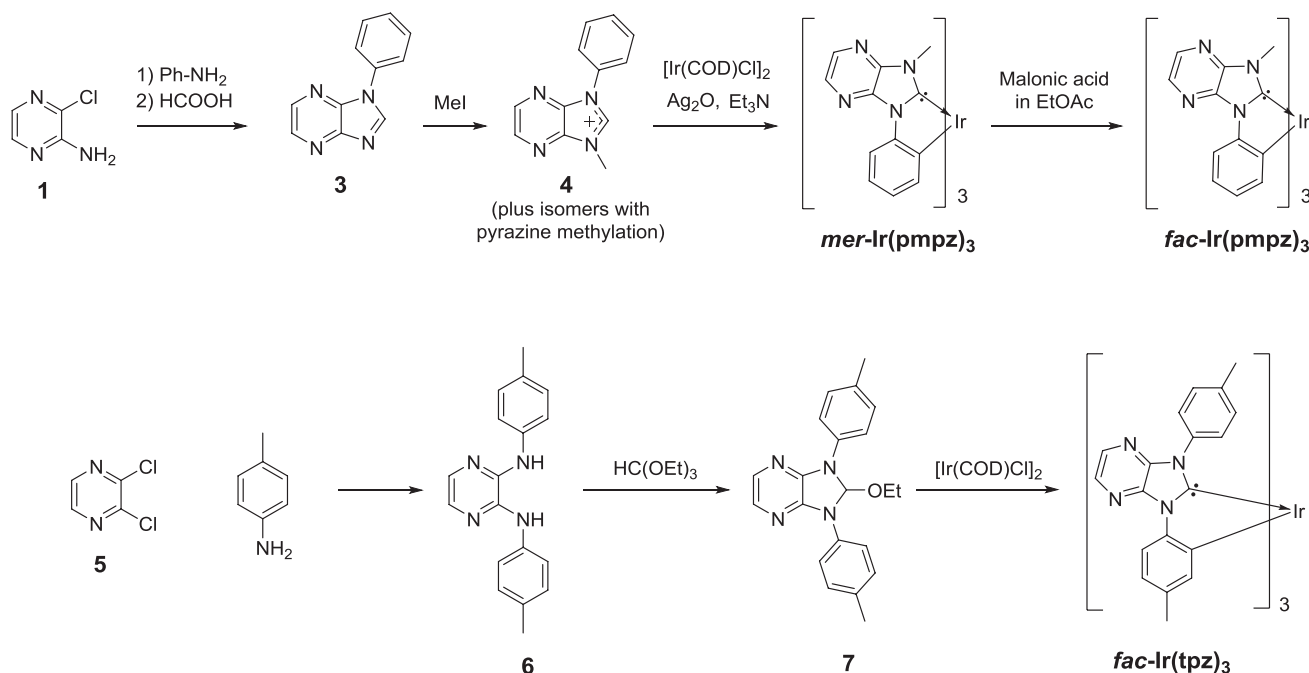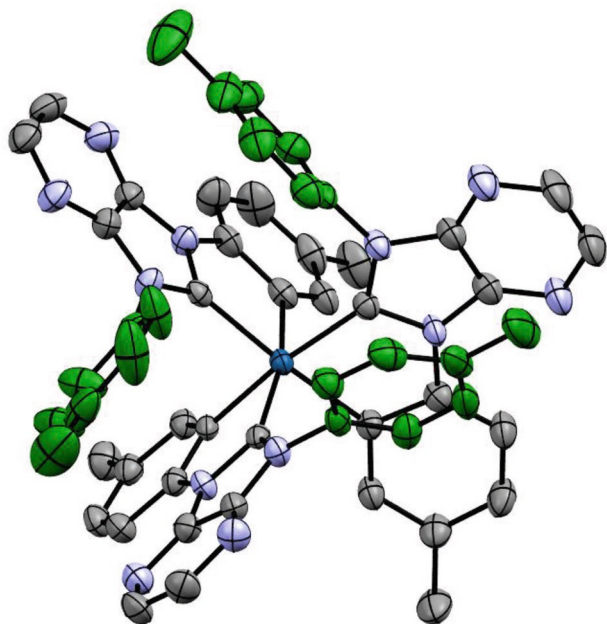
(pmp) to create highly efficient deep blue facial (fac) and meridional (mer) Ir complexes [Ir(pmp)$_3$] (**Scheme 1**).[1] Since this report, several analogues of these compounds have been reported.[12,14] OLEDs employing fac- and mer-Ir(pmp)$_3$ as deep blue emitters have achieved external efficiencies of 15%. However, due to their high triplet energies, these emitters could only be doped into inherently unstable phosphine oxide-based host materials, leading to short device lifetimes. Additionally,

Scheme 2. Synthesis of fac-Ir(pmpz)$_3$ and fac-Ir(tpz)$_3$.

**ADVANCED
SCIENCE NEWS**

www.advancedsciencenews.com

**ADVANCED
OPTICAL
MATERIALS**

www.advopticalmat.de

Figure 1. Thermal ellipsoid plot of *fac*-Ir(tpz)₃ from the single crystal X-ray structure. Nonmetalated tolyl groups are shown in green to highlight their orientation relative to the imidazolyl carbene of an adjacent ligand. The dihedral angles between the nonmetalated tolyl and imidazolyl group it is bound to are 60°, 73°, and 85° for the three ligands. Hydrogen atoms were omitted for clarity.

ligand on iridium using Ir(COD)₂Cl₂—to obtain exclusively *mer*-Ir(pmpz)₃, albeit at low yield. This meridional isomer can be converted to *fac*-Ir(pmpz)₃ through acid induced isomerization.[29] To our surprise, about 50% of *mer*-Ir(pmpz)₃ isomerizes into *fac*-Ir(pmpz)₃ during thermal heating under vacuum (see Figure S29, Supporting Information). To the best of our knowledge, this is the first thermal isomerization of Ir(C^C:)₃ complexes reported. The overall yields of *mer*-Ir(pmpz)₃ and *fac*-Ir(pmpz)₃ were 9% and 2%, respectively. Due to the low overall yield of the Ir(pmpz)₃ complexes, we targeted the more synthetically accessible isoelectronic complex, Ir(tpz)₃. As depicted in Scheme 2, the first step of Ir(tpz)₃ synthesis is a coupling reaction between 2,3-dichloropyrazine and toluidine to give diamino pyrazine, **6**, which is cyclized with triethyl orthoformate to obtain the final ligand, **7**. Unlike the reaction using the pmpz ligand, cyclometalation of the tpz ligand onto iridium led only to *fac*-Ir(tpz)₃. The exclusive formation of the facial isomer using the tpz ligand is presumably due to unfavorable interligand steric interactions in the meridional form. The overall yield of the three-step process for preparing *fac*-Ir(tpz)₃ is 18%. The *fac*-Ir(tpz)₃ complex is found to be remarkably stable as sublimation yields of 95% were achieved with no accompanying decomposition products.
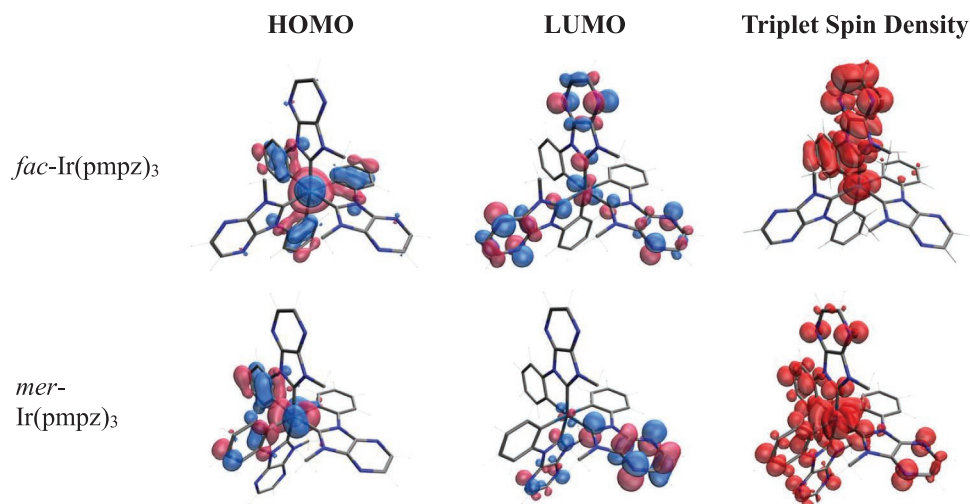
Single crystals of *fac*-Ir(tpz)₃ (**Figure 1**) were grown in methanol/dichloromethane solution and characterized using X-ray crystallography. The details of the structure solution, crystal data, atomic coordinates, bond lengths, and angles are reported in the Supporting Information and the structure has been deposited in the Cambridge Crystallographic Database (CCDC identifier: IMENIA). The geometry around the iridium atom is

pseudo-octahedral, with bond lengths and angles in the range reported for other Ir(C^C:)₃ complexes.[12,16,21,22] The Ir—C_(carbene) and Ir—C_(tolyl) bonds in the tpz ligands have effectively the same length, i.e., 2.027(2) and 2.087(2)–2.096(2) Å, respectively (data are provided in the Supporting Information). The Ir—C_(carbene) bond lengths in *fac*-Ir(tpz)₃ are similar to values found in other *fac*-Ir(C^C:) complexes, such as *mer*-Ir(pmb)₃ and *fac*-Ir(pmb)₃ derivatives.[16,21] Additionally, the Ir—C_(carbene) bond lengths in *fac*-Ir(tpz)₃ are similar to those found in *mer*-Ir(C^C:)₃ complexes (2.023(3)–2.054(9) Å).[12,22] The metalated tolyl rings are twisted from planarity around the bridging C_aryl—N_carbene bond, with dihedral angles averaging ≈7° between the arene and imidazolyl planes. This distortion of the C^C: ligand is also observed in *fac*-Ir(pmb)₃, where the twist is driven by steric interactions between hydrogen atoms on the benzimidazolyl carbene and metalated phenyl of the pmb ligand.[16] It is worth noting that the distortion in *fac*-Ir(tpz)₃ is roughly 5° larger than *fac*-Ir(pmb)₃, likely due to the addition of the bulky tolyl group. The nonmetalated tolyl groups are nearly parallel to the pyrazino-imidazolyl moiety of an adjacent tpz ligand (Figure 1), with closest atom–atom spacing of 3.2 Å.

The pendent non-metalated tolyl groups of *fac*-Ir(tpz)₃ are fluxional, as resonances for these aromatic protons are not observed in the ¹H NMR spectra taken at room temperature. This behavior is indicative of rapid rotation of the tolyl groups in fluid solution. Upon cooling to −40 °C, four distinct aromatic resonances appear as doublets between 6 and 7 ppm (see the Supporting Information), as would be expected on the basis of the crystal structure. The *ortho*-protons on the non-metalated tolyl group are inequivalent in the static structure as are the two *meta*-protons. The intensities of the tolyl aromatic protons decrease with increasing temperature as rotation of the pendent tolyl group accelerates and the signals coalesce at near room temperature. At higher temperature, the rotation the tolyl group becomes fast enough that two distinct proton resonances appear, with different resonances for the rapidly exchanging *ortho*- and *meta*-protons.

Several aspects of the reactivity of the Ir(C^C:)₃ complexes lend credence to the supposition that the metal–carbene linkage confers enhanced stability to these complexes over their Ir(C^N:)₃ congeners. Mass spectra taken of *fac*-Ir(pmpz)₃ and *fac*-Ir(tpz)₃ display peaks only for their parent ion; no peaks from molecular fragments are observed. In contrast, mass spectra of *fac*-Ir(C^N:)₃ complexes show multiple fragment peaks caused by loss of the C^N: ligand, with little or no parent molecular ion.[30,31] This behavior is consistent with a strong bond between the carbene ligand and the metal ion in the Ir(C^C:)₃ complexes. However, mass spectra of *mer*-Ir(pmpz)₃ do show fragment peaks with m/z = 285 and 611 amu suggesting that the C^C: ligands of *mer*-Ir(pmpz)₃ are less tightly bound than in the corresponding facial isomer.

Instability of Ir(C^N:)₃ complexes, particularly during use as a luminescent dopant in OLEDs, can be correlated with their propensity to thermally react with a chemical trap.[32–35] To further test the stability of the Ir(C^C:)₃ complexes, thermal substitution experiments were performed on *fac*-Ir(C^C:)₃ utilizing an N^N bidenate ligand (bathophenanthroline, BPhen) as a chemical trap.[33] BPhen readily binds to iridium complexes upon loss of chelated ligands. For these experiments, thin films comprised

**ADVANCED
SCIENCE NEWS**

www.advancedsciencenews.com

**ADVANCED
OPTICAL
MATERIALS**

www.advopticalmat.de

Figure 2. DFT (singlet and triplet, spin density, HOMO, and LUMO surfaces) of *fac*- and *mer*-Ir(pmpz)$_3$.

of a 1:1 mixture of *fac*-Ir(tpz)$_3$ and Bphen were heated at 100 °C. Films of FIrpic:Bphen and *fac*-Ir(ppy)$_3$:Bphen (both 1:1) were prepared and subjected to the same conditions for comparison (see the Supporting Information for details). Luminescence spectra taken of *fac*-Ir(tpz)$_3$:Bphen films after thermal aging for 2 days remained nearly identical to the spectra of pristine films (see the Supporting Information). Furthermore, no signal corresponding to Ir(tpz)$_2$BPhen complex was observed in the mass spectrum, suggesting that the tpz ligand was not displaced during this thermal aging process. In contrast, emission spectra of FIrpic and *fac*-Ir(ppy)$_3$ were redshifted and dramatically broadened upon thermal stress, consistent with displacement of picolinate (in FIrpic) and phenylpyridine [in *fac*-Ir(ppy)$_3$] ligands to form BPhen adducts of these complexes. Peaks corresponding to these BPhen adducts were subsequently identified using mass spectrometry (see the Supporting Information for experimental details). A parallel experiment was also performed by irradiating films having the same Ir complex:BPhen composition with 365 nm light for 48 h. Analysis of the irradiated films using mass spectroscopy showed FIrpic and *fac*-Ir(ppy)$_3$ formed the same adducts with BPhen as observed in the thermal degradation studies but no adducts were formed using *fac*-Ir(tpz)$_3$ (see the Supporting Information). This divergent reactivity further supports the presence of a strong bond between the carbene ligand and the metal ion in *fac*-Ir(tpz)$_3$, and hence its chemical robustness.

2.1.1. Computational Studies

Density functional theory (DFT) and time dependent DFT (TD-DFT) calculations were carried out to aid in evaluation of the electronic properties of the *fac*- and *mer*-Ir(C^C:)$_3$ complexes. The three highest occupied molecular orbitals (HOMO, HOMO–1, and HOMO–2) have electron densities localized on the Ir atom and metalated phenyl rings, whereas the three lowest unoccupied molecular orbitals (LUMO, LUMO+1, LUMO+2) are near degenerate and confined to the pyrazinoimidazolyl moieties and Ir center. Representative HOMO, LUMO, and triplet spin density surfaces for *fac*- and *mer*-Ir(pmpz)$_3$ are illustrated in **Figure 2**, energies for these valence orbitals, as well as the lowest singlet and triplet states are listed in **Table 1**. The HOMO and LUMO of *fac*-Ir(pmpz)$_3$ and *fac*-Ir(tpz)$_3$ are stabilized relative to *fac*-Ir(pmp)$_3$. The LUMO in the pyrazino derivatives is more stabilized than the HOMO, consequently decreasing the singlet and triplet energies.

The overlap between the HOMO and LUMO of the meridional isomers of the Ir(C^C:)$_3$ complexes is minimal, resulting in a smaller oscillator strength than for the facial isomers (Table 1). The weaker orbital overlap also gives rise to a decrease in the energy gap between the singlet and triplet excited states (ΔE_{ST}) for the meridional isomers relative to their facial counterparts. The orbital overlaps for the excited states of the facial and

Table 1. Calculated energies for frontier orbitals, singlet and triplet transitions (in eV) and dipole moments (in Debye) for the Ir(C^C:)$_3$ complexes from DFT and TD-DFT calculations (B3LYP/LACVP**).

	HOMO	LUMO	S_1, f[a]	T_1	ΔE_{ST}	Λ[b] S_1/T_1	μ S_0/T_1	μ'[c]	$\Delta\mu'$[d]
fac-Ir(pmp)$_3$	−4.97	−1.14	3.23, 0.0413	3.04	0.19	0.39/0.59	11.5/8.4	4.2	7.3
fac-Ir(pmpz)$_3$	−5.28	−1.80	2.90, 0.0355	2.69	0.21	0.35/0.58	7.1/11.3	−2.5	9.6
fac-Ir(tpz)$_3$	−5.03	−1.61	2.85, 0.0386	2.65	0.20	0.36/0.56	7.7/2.3	−2.2	9.9
mer-Ir(pmp)$_3$	−4.84	−1.28	2.99, 0.0045	2.93	0.06	0.28/0.44	7.4/11.4	−10.6	18.0
mer-Ir(pmpz)$_3$	−5.13	−1.92	2.65, 0.0027	2.60	0.05	0.24/0.41	4.5/18.2	−17.3	21.8

[a]f = oscillator strength; [b]Overlap integrals for the hole and electron NTOs; [c]Projection of the dipole moment vector of the T_1 state onto S_0 state. Positive values indicate the dipoles for each state are oriented in the same direction, whereas negative values indicate they oppose each other; [d]Change in the dipole moment between $\mu(S_0)$ and μ'.

meridional isomers were quantified by calculating the extent of spatial overlap (Λ) between the hole and electron natural transition orbitals (NTOs) for transitions associated with the S_1 and T_1 states (Table 1, see the Supporting Information for details on the method). The S_1 state gives a lower Λ value than that of the T_1 for a given Ir(C^C:)$_3$ compound, due to slightly differing nature of the S_1 and T_1 states. The S_1 state has a predominant metal-to-ligand charge transfer (MLCT) character, whereas the T_1 state has significant ligand centered (π–π^*) character mixed in. The Λ values are markedly lower for the meridional isomers than their facial counterparts. The value of Λ will approach unity for strongly localized excitations, such as in π–π^* transitions with substantial spatial overlap and zero for purely charge transfer (CT) transitions with no spatial overlap. For example, the computed Λ value and experimental S_1–T_1 gap for anthracene, a compound with a localized π–π^* transition, are $\Lambda = 0.84$ (S_1) and 0.89 (T_1), $\Delta E_{ST} = 1.46$ eV,[36] whereas a compound with a CT excited state, e.g., 2,4,5,6-tetrakis(carbazol-9-yl)-1,3-dicyanobenzene (4CzIPN) gives $\Lambda = 0.29$ (S_1) and 0.32 (T_1) and $\Delta E_{ST} = 0.10$ eV.[37,38] More relevant are values for fac-Ir(ppy)$_3$: $\Lambda = 0.46$ (S_1) and 0.69 (T_1), $\Delta E_{ST} = 0.48$ eV.[39] It is evident that the Λ and ΔE_{ST} values for the Ir(C^C:)$_3$ complexes, particularly the meridional isomers, suggest they have pronounced CT character in their excited states. Moreover, the dipole moments calculated for the optimized S_0 and T_1 states of the mer-isomers undergo a larger change than for the fac-isomers. The magnitude for the change falls between 7.3 and 9.9 D for the fac-isomers, whereas the values are 18.0 and 21.8 D for mer-Ir(pmp)$_3$ and mer-Ir(pmpz)$_3$, respectively (Table 1; and Figure S23, Supporting Information).

2.1.2. Electrochemical and Photophysical Properties

The electrochemical properties of the Ir(C^C:)$_3$ complexes were analyzed using cyclic voltammetry (CV) and differential pulse voltammetry (DPV) (see the Supporting Information for traces). The complexes display a single quasi-reversible oxidation, with the potentials of mer-complexes being 250 mV lower than their fac-counterparts. Three closely spaced, reversible reduction waves are observed for the Ir(C^C:)$_3$ complexes. The greater electronegativity of the nitrogen atom versus methene (CH) lowers the first reduction potentials of fac-Ir(pmpz)$_3$ and fac-Ir(tpz)$_3$ by 600 mV relative to fac-Ir(pmp)$_3$, whereas the oxidation potentials differ by only 200 mV. The separation between the first and second reduction waves in fac-Ir(pmp)$_3$ (120 mV) and fac-Ir(pmpz)$_3$ (140 mV) is less than that for the first and second reduction in fac-Ir(ppy)$_3$ (300 mV),[39] indicating weaker interligand electronic coupling in the Ir(C^C:)$_3$ complexes than in the Ir(C^N:)$_3$ counterparts. The measured redox potentials (**Table 2**) correlate well with results from DFT calculations, which suggest that the HOMO energies of the meridional isomers are shallower than those of the facial isomers, whereas the LUMO energies are comparable.

The UV–visible absorption spectra of fac- and mer-Ir(pmp)$_3$, fac- and mer-Ir(pmpz)$_3$, and fac-Ir(tpz)$_3$ are shown in **Figure 3**. Strong absorption bands at high energy ($\lambda < 350$ nm) are assigned to ligand π–π transitions, whereas bands at lower energies are assigned to spin allowed MLCT transitions. The

Table 2. Electrochemical properties of the Ir(C^C:)$_3$ complexes.

| Complex	E_{ox} [V][a]	E_{red} [V][a]	ΔE_{redox} [V]
fac-Ir(pmp)$_3$	+0.60	−2.81, −3.03, −3.21	3.41
fac-Ir(pmpz)$_3$	+0.80	−2.21, −2.35, −2.52	3.01
fac-Ir(tpz)$_3$	+0.66	−2.14, −2.32, −2.50	2.80
mer-Ir(pmp)$_3$	+0.38	−2.78, −2.99, −3.18	3.16
mer-Ir(pmpz)$_3$	+0.55	−2.21, −2.36, −2.52	2.76

[a]Peak potentials determined using DPV measured in DMF with 0.1 M TBAF and referenced to an internal ferrocenium/ferrocene. couple.

absorption bands for the MLCT transitions in the facial isomers have relatively high extinction coefficients ($\varepsilon \approx 2.0 \times 10^4$ M^1 cm^1). These MLCT transitions in fac-, mer-Ir(pmpz)$_3$ and fac-Ir(tpz)$_3$ complexes are lower in energy ($\lambda = 400$–425 nm) than similar transitions in mer- and fac-Ir(pmp)$_3$ ($\lambda = 350$–380 nm).[1] The bathochromic shifts are consistent with the smaller ΔE_{redox} gaps in the complexes with pyrazino moieties compared to the analogs with the pmp ligand. The ^{1}MLCT transitions of the meridional isomers have lower extinction coefficients than their facial counterparts, as predicted by the TD-DFT calculations, consistent with poor orbital overlap between the HOMO and LUMO.

Photoluminescence (PL) spectra of the complexes were measured in 2-MeTHF and polystyrene (PS) and shown in **Figure 4**; the photophysical parameters are summarized in **Table 3**. PL spectra and data in other solvents and in PMMA films are given in the Supporting Information. The emission lifetimes (τ) were obtained from monoexponential fits to the data at room temperature. Radiative (k_r) and nonradiative (k_{nr}) rate constants are calculated from the emission lifetimes and Φ_{PL} using the relationship $k_r = \Phi_{PL}/\tau$, where $\Phi_{PL} = k_r/(k_r + k_{nr})$. The emission spectra of the Ir(pmpz)$_3$ complexes are redshifted compared to the emission spectra of the Ir(pmp)$_3$ complexes in all media.[1] The fac-Ir(tpz)$_3$ complex displays similar PL spectra with fac-Ir(pmpz)$_3$, but with a further redshift of 5 nm as a result of electron donation by the methyl group meta to iridium. Similar to mer-Ir(pmp)$_3$, the PL spectrum of mer-Ir(pmpz)$_3$ is broad and exhibits a large bathochromic shift relative to the fac-isomer. The broadened emission of mer-Ir(pmpz)$_3$ suggests
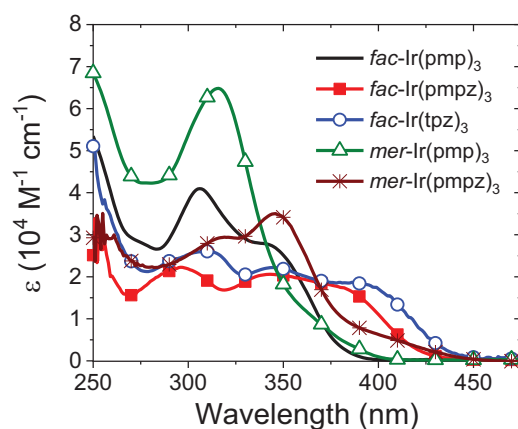
Figure 3. Absorption spectra of Ir(C^C:)$_3$ complexes in 2-MeTHF at 298 K.
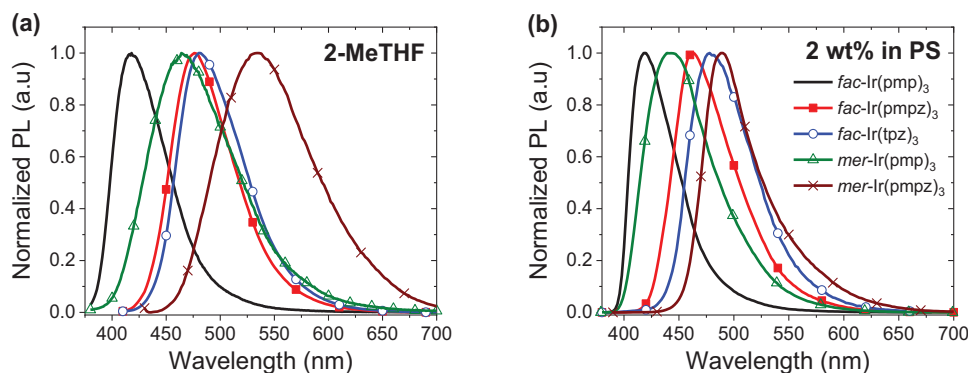
Figure 4. Emission spectra of Ir(C^C:)$_3$ complexes in a) 2-MeTHF at 298 K and b) PS at 298 K.

that the excited-state geometry is significantly distorted from that of the ground state. The decrease in emission energy of *mer*-Ir(pmpz)$_3$ compared to its facial isomer parallels its lower ΔE_{redox} gap and correspondingly smaller energy gap.

The complexes have high PL efficiencies in nonpolar solvents ($\Phi_{PL} > 0.65$). Emission in polar solvents is markedly red-shifted and accompanied by a decrease in the PL efficiency, especially for *mer*-Ir(pmpz)$_3$, (e.g., $\lambda_{em} = 495$ nm, $\Phi_{PL} = 76\%$ in cyclohexane; $\lambda_{em} = 590$ nm, $\Phi_{PL} = 0.8\%$ in acetonitrile; see the Supporting Information). This red-shift and drop in PL efficiency with solvent polarity is in contrast with the PL properties of *fac*-Ir(ppy)$_3$ which are relatively insensitive to solvent composition.[40] The solvatochromism of *fac*-Ir(pmpz)$_3$ is indicative of a pronounced charge transfer character in the Ir(C^C:)$_3$ complexes as reflected in the low values for the overlap integrals calculated for their S$_1$ states and consistent with the large change in dipole moment calculated for the T$_1$ state (Table 1). The decrease in PL efficiency with emission energy is caused

by an increase in the nonradiative rate constant, consistent with energy gap law (Figure S4, Supporting Information).[3] The emission spectra blue-shift and narrow in a rigid matrix (PS) and the luminescence efficiency increases (Φ_{PL} as high as 92%) as the k_{nr} of all the complexes is suppressed. The k_r of the meridional isomers in PS are some of the highest reported for Ir-based phosphors. As observed with *mer*-Ir(pmp)$_3$ in PS film, *mer*-Ir(pmpz)$_3$ has a shorter emission lifetime ($\tau = 0.93$ µs) than its facial isomer ($\tau = 2.50$ µs), owing to having a higher radiative rate constant ($k_r = 9.16 \times 10^5$ s^{-1} vs 3.44×10^5 s^{-1} for the facial isomer), despite also having a faster nonradiative rate ($k_{nr} = 1.62 \times 10^5$ s^{-1} vs $k_{nr} = 0.56 \times 10^5$ s^{-1} for the facial isomer). The unusually high k_r values of the meridional isomers could be related to their small singlet-triplet gaps ($\Delta E_{ST} \approx 0.05$ eV, based on TD-DFT).[41] Unusually high k_r values were not observed with the facial isomers as they have larger exchange energies ($\Delta E_{ST} \approx 0.2$ eV). Interestingly the emission lifetimes of all the complexes at $T = 77$ K remained relatively short.

Table 3. Photophysical properties of Ir(C^C:)$_3$ complexes in 2-MeTHF and polystyrene (PS).

complex	298 K					77 K	
	λ_{max} [nm]	Φ_{PL} [%]	τ [µs]	k_r [10^5 s^{-1}]	k_{nr} [10^5 s^{-1}]	λ_{max} [nm]	τ [µs]
2-MeTHF							
fac-Ir(pmp)$_3$	417	76	1.2	6.4	2.0	393	3.9, 9.2
fac-Ir(pmpz)$_3$	475	87	2.5	3.5	0.52	447	7.5
fac-Ir(tpz)$_3$	481	98	2.0	4.9	0.10	458	4.4
mer-Ir(pmp)$_3$	465	78	0.80	10	2.7	413	1.0
mer-Ir(pmpz)$_3$	530	27	0.44	6.2	17	490	2.0
2 wt% polystyrene							
fac-Ir(pmp)$_3$	420	78	1.1	7.1	2.00	–	3.3
fac-Ir(pmpz)$_3$	460	86	2.5	3.4	0.56	–	5.0
fac-Ir(tpz)$_3$	480	92	2.1	4.5	0.29	–	4.0
mer-Ir(pmp)$_3$	440	80	0.64	13	3.1	–	1.1
mer-Ir(pmpz)$_3$	490	85	0.93	9.2	1.6	–	1.7
Host	*fac*-Ir(tpz)$_3$ doped in EL host at 10%						
*m*CBP[a]	478	90	1.85	4.9	0.50	–	–
txl[b]	488	88	1.89	4.7	0.59	–	–

[a]*m*CBP = 3,3′-di(9*H*-carbazol-9-yl)-1,1′-biphenyl; [b]txl = 1-(4-(dibenzo[*b,d*]thiophen-4-yl)-2,5-dimethylphenyl)-1*H*-phenanthro[9,10-*d*]imidazole.
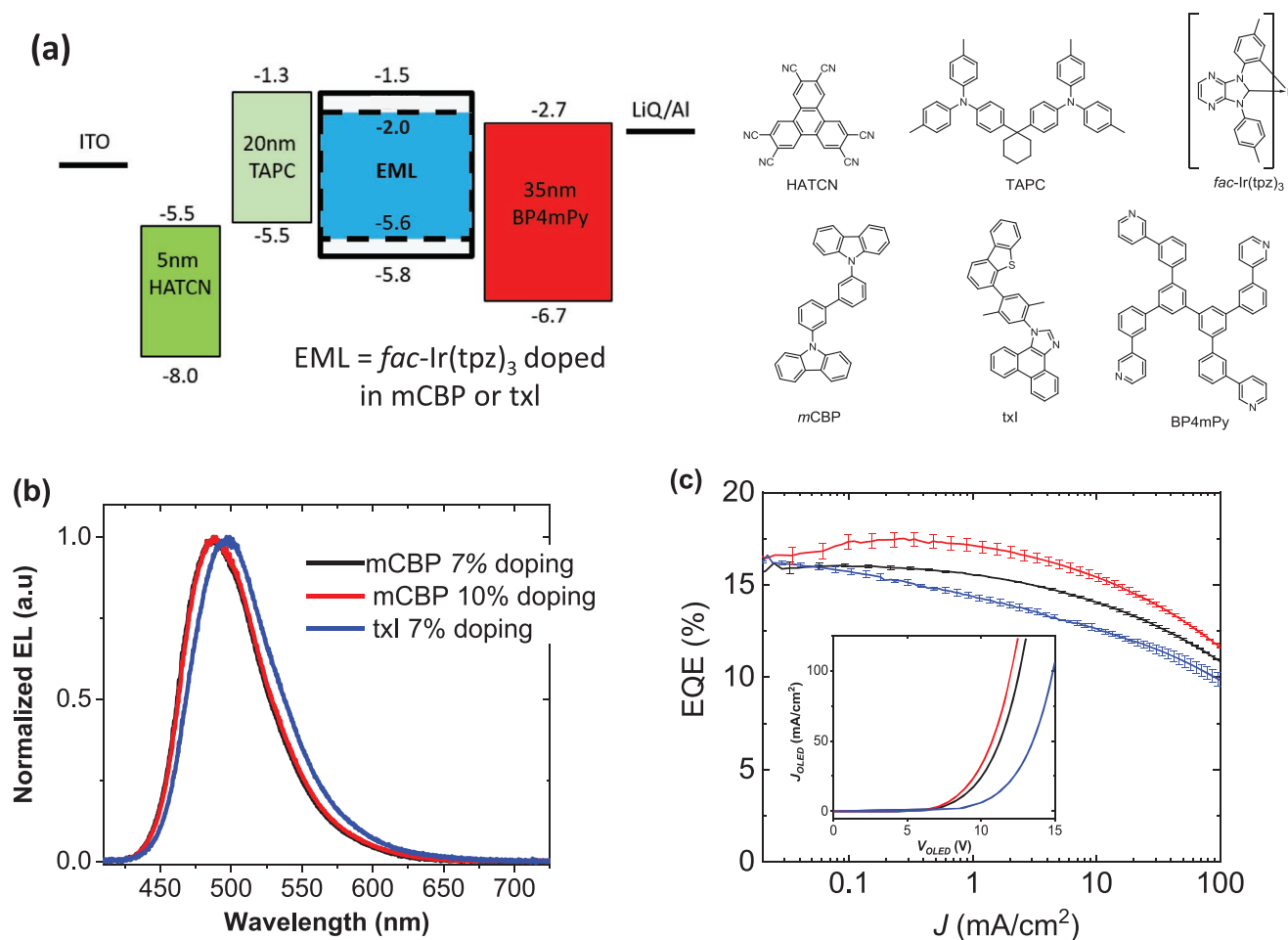
Figure 5. a) Device architecture of *fac*-Ir(tpz)$_3$-based OLEDs, with HOMO/LUMO energies given in eV. b) Electroluminescence spectra and c) current density–voltage (inset) and EQE curves for the devices.

2.1.3. Electroluminescence Properties

Blue emission with high luminance efficiency and scalable and high yielding synthesis make *fac*-Ir(tpz)$_3$ an ideal phosphorescent dopant for fabrication of blue OLEDs. The triplet energy for *fac*-Ir(tpz)$_3$ is slightly lower than *fac*-Ir(pmpz)$_3$, which allows it to be efficiently hosted in the stable host material 3,3′-di(9*H*-carbazol-9-yl)-1,1′-biphenyl (*m*CBP) where the photoluminescence efficiency remains high (Table 3). Additionally, the energy of the LUMO (2.3 eV) is similar to that of common electron

transport materials, facilitating electron injection and transport in the devices. The electroluminescence (EL) properties were investigated by fabricating OLEDs using *fac*-Ir(tpz)$_3$ as an emissive dopant using the device architecture shown in **Figure 5**. The choice of hole and electron transport materials was based on our previous success with these materials in blue phosphorescent OLEDs.[7] The OLED performance parameters are given in **Table 4** and plots of device efficiencies versus luminance are given in the Supporting Information. In these devices, *fac*-Ir(tpz)$_3$ was used as a blue dopant in an emissive layer comprised of *m*CBP

Table 4. OLED performance parameters for *fac*-Ir(tpz)$_3$ based OLEDs.

Host/doping level[a]	V_{on} [V]	L_{max} [cd m^{-2}]	EQE$_{max}$ [%]	CE$_{max}$ [cd m^{-2}]	Efficiency at 1000 cd m^{-2}			λ_{max} [nm] (CIE)
					EQE [%]	CE [cd A^{-1}]	PE [lm W^{-1}]	
*m*CBP/7%	4.1	27 000	15	33	14	32	4.3	488 (0.16, 0.38)
*m*CBP/10%	3.9	29 000	18	38	16	36	5.1	488 (0.16, 0.38)
txl/7%	4.2	24 000	16	38	13	32	3.5	497 (0.18, 0.45)
*m*CBP/8% Firpic[7]	3.3	28 000	17	40	16	39	5.8	475, 502[b] (0.15, 0.29)

[a]V_{on} = voltage at 1 cd m^{-2}, L = luminance, CE = current efficiency, PE = power efficiency; [b]The FIrpic EL spectrum in *m*CBP consists of two roughly equal intensity peaks.[7]

as well as another high triplet energy host 1-(4-(dibenzo[*b,d*]thiophen-4-yl)-2,5-dimethylphenyl)-1*H*-phenanthro[9,10-*d*]imidazole (txI).[7] The electroluminescence spectra of *fac*-Ir(tpz)$_3$ in the devices are very similar to their PL spectra in thin films, indicating effective exciton confinement on the dopant. Current density–voltage (*J*–*V*) measurements show that the conductivity of devices are independent of doping concentration in *m*CBP, but varies between the two hosts, suggesting that charges are also carried by the host materials. The maximum efficiency (18 ± 1%) was achieved in the optimized *m*CBP device and all of the devices give minimal efficiency decreases at high brightness (1000 cd m^{-2}). Devices with FIrpic in an identical architecture show similar electroluminescence and device performance at both low and high brightness levels.[7] Similar high efficiencies, in the 15–20% range without outcoupling enhancement are not common, but have been observed for OLEDs based on other Ir(C^C)$_3$ and Ir(C^N)$_3$ phosphors.[7,13,20,26,42–49]

3. Conclusion

In this work, we developed three new tris-Ir(III) carbene complexes featuring pyrazinoimidazolyl cyclometalating ligand (*fac*- and *mer*-Ir(pmpz)$_3$ and *fac*-Ir(tpz)$_3$) for use as blue dopants in OLEDs. Computational, electrochemical, and photophysical studies of these complexes along with the previously reported deep blue emitting tris-Ir(III) carbene complexes featuring pyridinoimidazolyl ligand (*fac*- and *mer*-Ir(pmp)$_3$) were carried out to interpret their excited state properties. The meridional isomers have minimal overlap between their HOMO and LUMO, resulting in a calculated energy difference between their singlet and triplet levels (ΔE_{ST}) that is small, and weak oscillator strengths for the lowest singlet states. The frontier orbitals of the facial isomers have larger overlap, leading to larger ΔE_{ST} and oscillator strengths than the meridional isomers. The HOMO (≈5.4 eV) and LUMO (≈2.1 eV) levels of the pyrazine analogs are ideal for charge injection into the EML. All of the reported complexes have high photoluminescence efficiencies (Φ_{PL} = 78–92%) in polystyrene matrices and nonpolar solvents; however, the efficiency decreases with increasing solvent polarity due to increase in nonradiative rates, consistent with the energy gap law.

Finally, *fac*-Ir(tpz)$_3$, the most promising complex was employed as a blue emissive dopant in OLEDs. Optimized blue phosphorescent OLEDs using this material achieved excellent electroluminescence efficiency (≈18 ± 1%), high brightness (29 000 cd m^{-2}) at low current density. Further substitution of the tpz ligand is being explored to generate a deep blue Ir(C^C:)$_3$ emitter.

Supporting Information

Supporting Information is available from the Wiley Online Library or from the author.

Conflict of Interest

Two of the authors (Prof. Forrest and Prof. Thompson) have a financial interest in one of the funders of this work (the Universal Display Corporation).

Data Availability Statement

Research data are not shared.

[1] J. Lee, H.-F. Chen, T. Batagoda, C. Coburn, P. I. Djurovich, M. E. Thompson, S. R. Forrest, *Nat. Mater.* **2016**, *15*, 92.

[2] M. E. Thompson, P. E. Djurovich, S. Barlow, S. Marder, in *Comprehensive Organometallic Chemistry*, Vol. *12* (Ed: D. O'Hare), Elsevier, Oxford **2007**, p. 101.

[3] J. V. Caspar, T. J. Meyer, *J. Phys. Chem.* **1983**, *87*, 952.

[4] T. Sajoto, P. I. Djurovich, A. B. Tamayo, J. Oxgaard, W. A. Goddard, M. E. Thompson, *J. Am. Chem. Soc.* **2009**, *131*, 9813.

[5] H. Yersin, A. F. Rausch, R. Czerwieniec, T. Hofbeck, T. Fischer, *Coord. Chem. Rev.* **2011**, *255*, 2622.

[6] M. Z. Shafikov, R. Daniels, V. N. Kozhevnikov, *J. Phys. Chem. Lett.* **2019**, *10*, 7015.

[7] M. Idris, C. Coburn, T. Fleetham, J. Milam-Guerrero, P. I. Djurovich, S. R. Forrest, M. E. Thompson, *Mater. Horiz.* **2019**, *6*, 1179.

[8] M. A. Baldo, S. Lamansky, P. E. Burrows, M. E. Thompson, S. R. Forrest, *Appl. Phys. Lett.* **1999**, *75*, 4.

[9] Y. Sun, X. Yang, Z. Feng, B. Liu, D. Zhong, J. Zhang, G. Zhou, Z. Wu, *ACS Appl. Mater. Interfaces* **2019**, *11*, 26152.

[10] Y. H. Sun, X. L. Yang, Z. Feng, B. A. Liu, D. K. Zhong, J. J. Zhang, G. J. Zhou, Z. X. Wu, *ACS Appl. Mater. Interfaces* **2019**, *11*, 26152.

[11] J. Lee, C. Jeong, T. Batagoda, C. Coburn, M. E. Thompson, S. R. Forrest, *Nat. Commun.* **2017**, *8*, 15566.

[12] Z. Chen, L. Wang, S. Su, X. Zheng, N. Zhu, C.-L. Ho, S. Chen, W.-Y. Wong, *ACS Appl. Mater. Interfaces* **2017**, *9*, 40497.

[13] S. Kim, H. J. Bae, S. Park, W. Kim, J. Kim, J. S. Kim, Y. Jung, S. Sul, S.-G. Ihn, C. Noh, S. Kim, Y. You, *Nat. Commun.* **2018**, *9*, 1211.

[14] B.-S. Yun, J.-H. Kim, S.-Y. Kim, H.-J. Son, D. W. Cho, S. O. Kang, *Phys. Chem. Chem. Phys.* **2019**, *21*, 7155.

[15] G. Sarada, A. Maheshwaran, W. Cho, T. Lee, S. H. Han, J. Y. Lee, S.-H. Jin, *Dyes Pigm.* **2018**, *150*, 1.

[16] T. Sajoto, P. I. Djurovich, A. Tamayo, M. Yousufuddin, R. Bau, M. E. Thompson, R. J. Holmes, S. R. Forrest, *Inorg. Chem.* **2005**, *44*, 7992.

[17] S. Haneder, E. Da Como, J. Feldmann, J. M. Lupton, C. Lennartz, P. Erk, E. Fuchs, O. Molt, I. Münster, C. Schildknecht, G. Wagenblast, *Adv. Mater.* **2008**, *20*, 3325.

**ADVANCED
SCIENCE NEWS**

www.advancedsciencenews.com

**ADVANCED
OPTICAL
MATERIALS**

www.advopticalmat.de

[18] C.-F. Chang, Y.-M. Cheng, Y. Chi, Y.-C. Chiu, C.-C. Lin, G.-H. Lee, P.-T. Chou, C.-C. Chen, C.-H. Chang, C.-C. Wu, *Angew. Chem., Int. Ed.* **2008**, *47*, 4542.

[19] C. Schildknecht, G. Ginev, A. Kammoun, T. Riedl, W. Kowalsky, H.-H. Johannes, C. Lennartz, K. Kahle, M. Egen, T. Geßner, M. Bold, S. Nord, P. Erk, *Proc. SPIE* **2005**, *5937*, 59370E.

[20] H. Sasabe, J.-i. Takamatsu, T. Motoyama, S. Watanabe, G. Wagenblast, N. Langer, O. Molt, E. Fuchs, C. Lennartz, J. Kido, *Adv. Mater.* **2010**, *22*, 5003.

[21] K. Tsuchiya, S. Yagai, A. Kitamura, T. Karatsu, K. Endo, J. Mizukami, S. Akiyama, M. Yabe, *Eur. J. Inorg. Chem.* **2010**, *2010*, 926.

[22] A. K. Pal, S. Krotkus, M. Fontani, C. F. R. Mackenzie, D. B. Cordes, A. M. Z. Slawin, I. D. W. Samuel, E. Zysman-Colman, *Adv. Mater.* **2018**, *30*, 1804231.

[23] Y.-J. Cho, S.-Y. Kim, J.-H. Kim, J. Lee, D. W. Cho, S. Yi, H.-J. Son, W.-S. Han, S. O. Kang, *J. Mater. Chem. C* **2017**, *5*, 1651.

[24] X. Zhou, B. J. Powell, *Inorg. Chem.* **2018**, *57*, 8881.

[25] S. Arroliga-Rocha, D. Escudero, *Inorg. Chem.* **2018**, *57*, 12106.

[26] A. Maheshwaran, V. G. Sree, H. Y. Park, H. Kim, S. H. Han, J. Y. Lee, S. H. Jin, *Adv. Funct. Mater.* **2018**, *28*, 1802945.

[27] M. Jung, K. H. Lee, J. Y. Lee, T. Kim, *Mater. Horiz.* **2020**, *7*, 559.

[28] K. D. Peter Murer, F. L. Benedito, G. Battagliarn, S. Metz, U. Heinmeyer, C. Lennartz, G. Wagenblast, S. Watanabe, T. Gessner, *World Patent Application WO2015000955A1*, BASF SE, Ludwigshafen, Germany **2015**.

[29] J. G. Osiak, T. Setzer, P. G. Jones, C. Lennartz, A. Dreuw, W. Kowalsky, H.-H. Johannes, *Chem. Commun.* **2017**, *53*, 3295.

[30] C. Jeong, C. Coburn, M. Idris, Y. Li, P. I. Djurovich, M. E. Thompson, S. R. Forrest, *Org. Electron.* **2019**, *64*, 15.

[31] S. Scholz, D. Kondakov, B. Lüssem, K. Leo, *Chem. Rev.* **2015**, *115*, 8449.

[32] M. J. Jurow, A. Bossi, P. I. Djurovich, M. E. Thompson, *Chem. Mater.* **2014**, *26*, 6578.

[33] M. Cazzaniga, F. Cargnoni, M. Penconi, A. Bossi, D. Ceresoli, *Chem. Mater.* **2019**, *31*, 2269.

[34] I. R. d. Moraes, S. Scholz, B. Lüssem, K. Leo, *Appl. Phys. Lett.* **2011**, *99*, 053302.

[35] I. R. de Moraes, S. Scholz, B. Lüssem, K. Leo, *Org. Electron.* **2012**, *13*, 1900.

[36] S. Schols, A. Kadashchuk, P. Heremans, A. Helfer, U. Scherf, *Proc. SPIE* **2009**, *7415*, 74150A.

[37] H. Nakanotani, K. Masui, J. Nishide, T. Shibata, C. Adachi, *Sci. Rep.* **2013**, *3*, 2127.

[38] Y. R. Cho, S. J. Cha, M. C. Suh, *Synth. Met.* **2015**, *209*, 47.

[39] A. B. Tamayo, B. D. Alleyne, P. I. Djurovich, S. Lamansky, I. Tsyba, N. N. Ho, R. Bau, M. E. Thompson, *J. Am. Chem. Soc.* **2003**, *125*, 7377.

[40] S. Takayasu, T. Suzuki, K. Shinozaki, *J. Phys. Chem. B* **2013**, *117*, 9449.

[41] D. S. M. Ravinson, M. E. Thompson, *Mater. Horiz.* **2020**, *7*, 1210.

[42] R. Hamze, M. Idris, D. S. Muthiah Ravinson, M. C. Jung, R. Haiges, P. I. Djurovich, M. E. Thompson, *Front. Chem.* **2020**, *8*, 401.

[43] H. Ma, D. Liu, J. Li, Y. Mei, D. Li, Y. Ding, W. Wei, *New J. Chem.* **2020**, *44*, 8743.

[44] H.-H. Kuo, Z.-l. Zhu, C.-S. Lee, Y.-K. Chen, S.-H. Liu, P.-T. Chou, A. K.-Y. Jen, Y. Chi, *Adv. Sci.* **2018**, *5*, 1800846.

[45] Y. Feng, X. Zhuang, D. Zhu, Y. Liu, Y. Wang, M. Bryce, *J. Mater. Chem. C* **2016**, *4*, 10246.

[46] K. Udagawa, H. Sasabe, F. Igarashi, J. Kido, *Adv. Opt. Mater.* **2015**, *4*, 86.

[47] K. Udagawa, H. Sasabe, C. Cai, J. Kido, *Adv. Mater.* **2014**, *26*, 5062.

[48] M. Sarma, W.-L. Tsai, W.-K. Lee, Y. Chi, C.-C. Wu, S.-H. Liu, P.-T. Chou, K.-T. Wong, *Chem* **2017**, *3*, 461.

[49] Y. Zhang, J. Lee, S. R. Forrest, *Nat. Commun.* **2014**, *5*.